UC Santa Barbara

UC Santa Barbara Previously Published Works

Title

Holocene Surface Rupture History of an Active Forearc Fault Redefines Seismic Hazard in Southwestern British Columbia, Canada

Permalink

https://escholarship.org/uc/item/7355n8px

Journal

Geophysical Research Letters, 45(21)

ISSN

0094-8276

Authors

Morell, KD
Regalla, C
Amos, C
et al.

Publication Date

2018-11-16

DOI

10.1029/2018gl078711

Peer reviewed

eScholarship.org Powered by the California Digital Library
University of California

Holocene surface rupture history of an active forearc fault redefines seismic hazard in southwestern British Columbia, Canada

K. D. Morell[1,2], C. Regalla[3], C. Amos[4], S. Bennett[5], L. Leonard[1], A. Graham[1], T. Reedy[6], V. Levson[1], A. Telka[7]

[1]School of Earth and Ocean Sciences, University of Victoria, Victoria, BC, Canada.
[2]Department of Earth Science, University of California, Santa Barbara, Santa Barbara, California, USA.
[3]Department of Earth and Environment, Boston University, Boston, Massachusetts, USA.
[4]Geology Department, Western Washington University, Bellingham, Washington, USA.
[5]U.S. Geological Survey, Menlo Park, California, USA.
[6]University of Nevada, Reno, USA.
[7]Paleotec Services, Ottawa, Ontario, Canada.

Key Points:

- We present the first surface rupture history of an onland forearc fault in British Columbia, Canada.
- The Leech river fault produced three surface-rupturing earthquakes in the last ∼9 kyr, and is capable of producing large earthquakes.
- The Canadian forearc likely contains additional active forearc faults that could host damaging surface-rupturing earthquakes.

Corresponding author: Kristin Morell, kmorell@ucsb.edu

Abstract

Characterizing the hazard associated with Quaternary-active faults in the forearc crust of the northern Cascadia subduction zone has proven challenging due to historically low rates of seismicity, late Quaternary glacial scouring, and dense vegetation that often obscures fault-related geomorphic features. We couple lidar topography with paleoseismic trenching across the Leech River fault on southern Vancouver Island to produce the first surface rupture history of an onland forearc fault in British Columbia, Canada. The results indicate that this fault produced three surface-rupturing earthquakes in the last ~9 kyr, and is therefore capable of producing large ($M_w > 6$) earthquakes in the future. We provide new constraints on the fault's length (~130 km) and Holocene slip rate (≥0.2-0.3 mm/yr) that, together with the earthquake ages, should be incorporated into new seismic hazard assessments and building code practices relevant to urban centers in southwestern British Columbia (Canada) and northwestern Washington state (USA).

1 Introduction

Recent earthquakes in Japan (April 2016 M_w 6.2 and M_w 7.0 Kumamoto (Hata, Goto, & Yoshimi, 2016) and April 2011 M_w 6.6 Iwaki (Toda & Tsutsumi, 2013)), Chile (March 2010 M_w 7.0 Pichilemu (Farías, Comte, Roecker, Carrizo, & Pardo, 2011)) and New Zealand (November 2016 M_w 7.8 Kaikoura (Bai, Lay, Cheung, & Ye, 2017)) highlight the damage that can be caused by strong to major (M_w > 6-7) forearc fault rupture, especially if the hypocenter is located near infrastructure and population. The April 2016 earthquake sequence located near Kumamoto, southwestern Japan (pop. ~740,000), was arguably the most damaging of these recent examples, resulting in at least 50 fatalities, 3,000 injuries, and US$1 billion in economic loss (Hata et al., 2016). Mitigating the damage caused by these types of events requires building code practices derived from seismic hazard assessments that incorporate the location, length, paleoseismic history, and/or slip rate of active forearc faults as discrete seismic sources (e.g. Youngs & Coppersmith, 1985).

In the northern Cascadia subduction zone in British Columbia, Canada (Fig. 1A), few Quaternary-active faults have been formally identified, due to low rates of instrumentally recorded seismicity (Balfour, Cassidy, Dosso, & Mazzotti, 2011), latest Quaternary glacial scouring of the landscape by the Cordilleran ice sheet until ~12,000 ^{14}C BP (Clague & James, 2002), and dense vegetation that often obscures fault-related geomorphologic features. Thus, the seismic hazard posed by active forearc faults to the growing population centers near this region (Fig. 1A) has yet to be robustly quantified.

Here we use lidar analysis and paleoseismic trenching across late Quaternary fault scarps along the Leech River fault (Morell, Regalla, Leonard, Amos, & Levson, 2017), a terrane-bounding structure on southern Vancouver Island (Fig. 1B), to produce the first surface rupture history of an onland forearc fault in British Columbia. We constrain the fault's location, orientation, and slip rate as first-order data necessary for probabilistic seismic hazard assessments (e.g. Halchuk, Allen, Adams, & Rogers, 2015). These assessments are critical for mitigating the impacts of future earthquakes on the infrastructure and population of greater Victoria (pop. ~250,000), the provincial capital located <5 km from the Leech River fault, as well as other population centers in northwest Washington and southwest British Columbia (Fig. 1). We suggest that the Leech River fault is likely one of a network of active faults that accommodate plate boundary strain in northern Cascadia, and the results reinforce that paleoseismic studies are essential in quantifying the seismic hazard posed by forearc faults worldwide.

2 Evidence for large, surface-rupturing earthquakes

To constrain the number and chronology of recent surface-rupturing earthquakes along the Leech River fault, we mapped the structures and geometry of bedrock and late Quaternary deposits in two paleoseismic trenches located ~25 km west of Victoria (Fig. 1B). Lidar topography (e.g. Nelson et al., 2003) and paleoseismic trenching (e.g. Wilson, Bartholomew, & Carson, 1979) have been used to constrain the rupture history of faults in the Cascadia forearc for several decades. We selected trench sites using field work and bare-earth lidar data (James, Bednarski, Rogers, & Currie, 2010), which reveal a linear, uphill-facing scarp cutting across a colluvial apron developed on glacial till (Fig. 2A). Several debris-flow channels incising into this colluvial apron exhibit ~3 m of vertical separation across this scarp (Fig. 2B). Larger magnitude vertical separation (~6 m) of adjacent interfluves suggest the scarp was formed by at least two surface-rupturing earthquakes since the formation of the colluvial apron following the last deglaciation ~12,000 ^{14}C BP (Morell et al., 2017). To test this hypothesis, we excavated two trenches across the scarp, one on the colluvial apron surface (trench 1, T1) and one in a debris-flow channel (trench 2, T2) (Fig. 2A) (see Supporting Information (SI) for trench logs, unit descriptions, and detailed methods (Bennett et al., 2018; McCalpin, 2009; Reitman, Bennett, Gold, Briggs, & DuRoss, 2015; Thompson et al., 2002)).

Observations from T1 confirm at least three surface-rupturing earthquakes occurred along this section of the Leech River fault in the late Quaternary (Fig. 3A). The most recent, event 1, is recorded in T1 by an undeformed <0.5 m thick colluvial wedge (unit 4), that caps a steep fault zone. Event 2, the penultimate earthquake, is marked by unit 3, a second colluvial wedge beneath unit 4 at the toe of the uphill-facing scarp. Event 1 placed stratigraphically lower units (e.g., till) over unit 3, rotated the long axes of several clasts in unit 3 sub-parallel to the steep fault zone, and produced ~70-80 cm of displacement (Figs. 3A, S1 and S2). The oldest earthquake recorded in T1, event 3, is demarcated by unit 2, a wedge-shaped deposit below unit 3 (Fig. 3A). Unit 2 is thickest (~1 m) above the fault zone, thins towards the toe of the scarp, and contains toppled blocks of till. The near-vertical orientation of clasts in unit 2, its steep fault-bounded northern margin, and faults that cut this unit but terminate at the base of overlying units, indicate that unit 2 was deformed by events 1 and 2. Unit 2 buries a paleosol (unit 1b) developed onto hillslope colluvium (unit 1a) that overlies lodgement till (unit 1) on the downthrown (southern) side of the fault (Fig. 3A). Unit 1 is displaced by a total of ~3 m across the ~20-50 cm wide scarp-forming fault zone, which contains sheared sediments and till.

Observations from T2, excavated ~20 m west of T1 (Fig. 2A), likewise indicate that this portion of the Leech River fault has hosted three surface-rupturing earthquakes in the late Quaternary. Event 1 is recorded in T2 by unit 6, an undeformed scarp-derived colluvium that overlies two main fault strands that terminate upwards into its basal contact (fault 1, F1; and fault 2, F2) (Fig. 3A). Event 2, which ruptured ~1 m along F2, produced unit 4 in T2, a ~40 cm thick colluvial wedge that lies stratigraphically below unit 6. Event 1 displaced the basal contact of unit 4 by 10-15 cm along F1 and 20-50 cm along F2, and rotated clasts in unit 4 to steep orientations, parallel to F2 (Figs. 3B, S3 and S4). Event 3 placed schist of the Leech River Complex (unit 1) in fault contact with late Quaternary loess deposits (unit 2) along F1. The topographic scarp produced by event 3 was removed in T2 due to debris-flow processes, including a highly erosive debris flow that produced a coarse debris-flow colluvium (unit 3). These debris-flow processes explain the ~3 m difference in vertical separation observed across the scarp between the debris-flow channel and colluvial apron surface (Fig. 2B).

3 Earthquake chronology, fault displacement and fault slip rate

To constrain the timing of the three earthquakes recorded in the trenches, we radiocarbon dated 51 fragments of charcoal sampled from Quaternary units in both trenches and used these ages to constrain the calendar age of each earthquake using OxCal software. OxCal uses a Bayesian statistical analysis and a Markov Chain Monte Carlo process to model the timing of past events as a probability distribution function (Bronk Ramsey, 2009; Lienkaemper & Ramsey, 2009). To calculate a minimum fault slip rate for use in probabilistic seismic hazard assessments (Youngs & Coppersmith, 1985), we used this earthquake chronology together with fault displacement estimates derived from stratigraphic offsets, colluvial wedge thicknesses, and total surface offsets (see SI for details).

We used 25 of the 51 radiocarbon ages from both trenches in a combined OxCal model to constrain earthquake ages to 1.7 ± 0.1, 2.2 ± 0.1, and 8.7 ± 0.3 thousand calendar years ago (hereafter abbreviated as ka) (Fig. 4). We included as many ages as possible in the OxCal model, excluding only the fewest number in order to maintain stratigraphic order between adjacent units. We assume that apparently young ages result from overlying roots or burrowing, whereas apparently old ages arise from recycling of older charcoal into younger units. For debris flow units, we assume that the youngest radiocarbon ages most closely represent the age of the deposit. The age of event 1 is constrained by ten minimum ages ranging from ∼1.7 to 0.4 ka and by five maximum ages spanning ∼2.2 to 1.7 ka (Fig. 4). The minimum age of event 2 is constrained by the five ∼2.2 to 1.7 ka samples and by four maximum ages ranging from ∼2.8 to 2.2 ka from the debris flow colluvium unit 3 in T2. The age of event 3 is bracketed by three minimum ages spanning from ∼8.5 to 6.9 ka and three maximum ages ranging from ∼10.9 to 8.9 ka (Fig. 4).

These earthquake ages together with fault displacement estimates suggest that this section of the Leech River fault has slipped at a rate of ≥0.2-0.3 mm/yr since ∼9 ka (Table 1). Stratigraphic offsets and colluvial wedge thicknesses indicate ∼1 m of displacement per event, and ∼3 m in cumulative displacement from all three events. Using vertical separation of the ground surface as a measure of fault displacement (e.g. Fig. 2B) yields a larger average cumulative displacement (∼5 m) (Morell et al., 2017) than total displacement estimates derived from stratigraphic offsets and colluvial wedge thicknesses (∼2-3 m). This discrepancy can be explained by distributed off-fault deformation and folding, and suggests that the slip rate calculations represent minimum estimates.

Holocene Fault Behavior

To place the trench results in a regional context, we measured the orientation of faults, structural fabrics, and kinematic indicators in the trenches, and mapped the surface geology of the surrounding colluvial apron. The trenches expose a ∼10-m-wide steep zone of distributed faults (Fig. 3A). The fault trace separating the Leech River Complex from the Metchosin Formation (Massey, MacIntyre, Desjardins, & Cooney, 2005) is located several meters south of the fault zone in the trenches (Fig. 2A). No topographic break occurs at this lithology-bounding fault, suggesting that it has not ruptured since the development of the colluvial apron surface.

The topography of the colluvial surface and fault slickenline data both indicate that all three events recorded in the trenches were dip-slip events. Neither the debris-flow channel walls nor the thalwegs show lateral offset (Fig. 2A), and slickenline data measured on faults that cut late-Quaternary sediments exhibit steep rake angles (∼70-90°; n=5, T2) (Fig. 3C). Whether these Holocene dip-slip earthquakes ruptured with normal or reverse motion remains somewhat ambiguous, however. In both trenches, the major faults and most minor structures are vertical to steeply south-dipping (>65° dip), suggestive of normal motion (Fig. 3A). But, fault G dips steeply north (285/67/N), and thrusts till

over colluvium in the west wall of T1. In contrast to the high rake angles measured on fault planes cutting Quaternary units, four of five slickenlines measured on bedrock-bedrock faults in T2 exhibited sub-horizontal rake angles ($< 10°$; Fig. 3B). This bimodal orientation of slickenlines implies a temporal switch in fault kinematics, which may be due to slip partitioning (e.g. McCaffrey, 1996), temporary changes in stress state during the megathrust seismic cycle (e.g. Toda & Tsutsumi, 2013), or variations in plate tectonic stresses or configurations over time (e.g. Bellier & Zoback, 1995).

Because Holocene activity of the Leech River fault would have significant implications for regional seismic hazards, it is important to ensure that the offsets in the trenches were produced by tectonic processes. Deep-seated landslides driven by gravity (sackungen) are often found in areas of high relief with recent glacial histories (McCalpin & Hart, 2002; Pánek & Klimeš, 2016; Tabor, 1971). These features typically manifest on steep slopes near ridge crests as swarms of scarps parallel to topographic contours. Several observations indicate that the offsets in the trenches were not produced by processes related to gravity. First, the Holocene offsets in the trenches occur far below (200 m) the nearest hill crest. Second, no additional scarps occur in the surrounding colluvial apron (Fig. 2A). Third, the trenches record three episodic, rather than gradual, pulses of deformation, which does not support formation by gravity creep. Finally, the fact that the earthquake ages are not clustered in time near ∼12,000 ^{14}C BP suggests that they were not produced due to stress release following the last deglaciation (Hetzel & Hampel, 2005).

Geological and geophysical data from previous studies suggest the Holocene fault zone exposed in the trenches extends for tens to hundreds of kilometers along strike to the east. Geologic mapping indicates that the faults in the trenches are part of a 100-500-m wide steep Quaternary-active fault zone that extends for ∼30 km eastward from the trench sites to the shoreline near Colwood (Fig. 1B) (Graham, 2018; Morell et al., 2017). Marine geophysical surveys by Barrie and Greene (2018) confirm that this fault system continues eastward for an additional ∼50 km offshore beneath the Juan de Fuca Strait to connect with the Holocene-active Darrington-Devil's Mountain fault zone of Washington state (Personius et al., 2014) (Fig. 1A). Collectively, these observations suggest that the active fault system in the trenches extends to the east for ∼130 km.

Implications for forearc seismic hazards and the need for paleoseismic studies

The results reinforce that paleoseismic studies are essential in identifying and quantifying the seismic hazard posed by forearc faults. Although the Leech River fault does not exhibit abundant instrumentally-recorded seismicity (Balfour et al., 2011), we show using paleoseismic trenching that this fault produced at least three surface-rupturing earthquakes in the last ∼9 kyr. Empirical relations between event magnitude and displacement (Wells & Coppersmith, 1994) suggest that each of the events were 6.5-6.7 in magnitude, given that each ruptured with ∼1 m of displacement. These results, together with the length of the fault zone (∼130 km) and Holocene slip rate (≥0.2-0.3 mm/yr), provide critical input for updating seismic hazard assessments and building practices relevant to the population of southwest British Columbia and northwest Washington (Fig. 1).

Given the active forearc setting, the Leech River and Darrington-Devil's Mountain faults (Fig. 1) are likely part of a network of Holocene-active faults that accommodate plate boundary strain in the forearc of northern Cascadia that have yet to be identified. Our study demonstrates that the Quaternary-active forearc fault system of Washington state (Fig. 1A) continues westward onland into Canada, and similar paleoseismic studies such as this one are needed to test if this fault system continues northward. The Boulder Creek (Sherrod et al., 2013) Holocene-active fault of Washington state lies only 30 km from the city of Vancouver, and the northward continuation of this fault system would

impact seismic hazard assessments relevant to the population and built infrastructure of the greater Vancouver region (pop. ∼3.5 million).

Active forearc regions contain some of the world's largest populations, including Tokyo (Japan, pop. ∼34 million), Mexico City (Mexico, pop. ∼9 million), Lima (Peru, ∼9 million) and Santiago (Chile, pop. ∼6 million). This study reinforces the need to use paleoseismic studies to update the potential seismic hazard caused by active forearc faults in these populated forearcs, even in regions with low seismicity rates. Considering that the meters-high fault scarps excavated for this study (Fig. 2) were concealed beneath tree cover prior to the acquisition of bare-earth lidar data (James et al., 2010; Morell et al., 2017), this study also confirms that lidar topography together with paleoseismic studies are crucial datasets in constraining the seismic hazards posed by forearc faults in heavily forested regions such as Cascadia.

Acknowledgments

Funding was provided by an NSERC Engage grant supported by the BC Hydro Electric Company, an NSERC Discovery grant to Morell, and NSF EAR IRFP Grant #1349586 to Regalla. We thank CRD Watersheds for access, Martin Lawrence of BC Hydro for his support, and Ray Wells, John Clague and Harvey Kelsey for discussions at the trench review. We thank Rich Briggs, Harvey Kelsey and an anonymous reviewer for their reviews. The data used are listed in the references, tables, and supplements. Any use of trade, product, or firm names is for descriptive purposes only and does not imply endorsement by the U.S. Government.

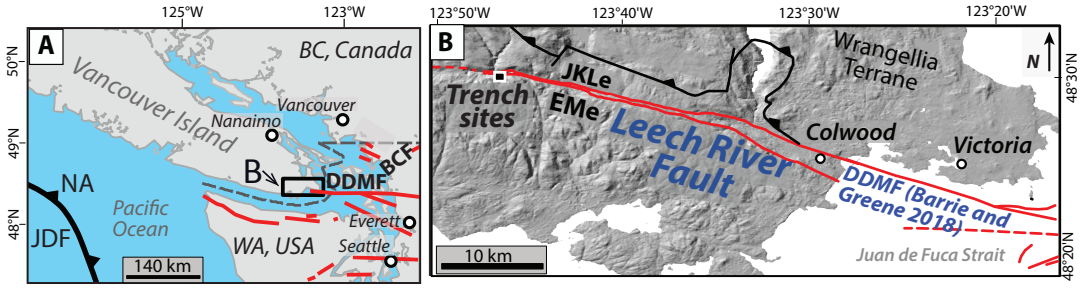

Figure 1. **A.** Regional setting showing simplified trace of forearc faults (in red) identified as Quaternary-active (Barrie & Greene, 2018; Nelson et al., 2017; Personius et al., 2014; USGS Quaternary fault and fold database for the United States, 2010) with respect to cities in British Columbia (BC), Canada, and Washington (WA), USA. Faults beneath the Pacific Ocean are not shown. Dashed line indicates Canada-USA international border. NA, North America plate; JDF, Juan de Fuca plate; DDMF, Darrington-Devil's Mountain fault; BCF, Boulder Canyon fault. **B.** Map of Leech River fault (Graham, 2018; Morell et al., 2017), trench sites, and the DDMF. EMe, Eocene Metchosin Fm; JKLe, Jurassic-Cretaceous Leech River Complex (Massey et al., 2005).

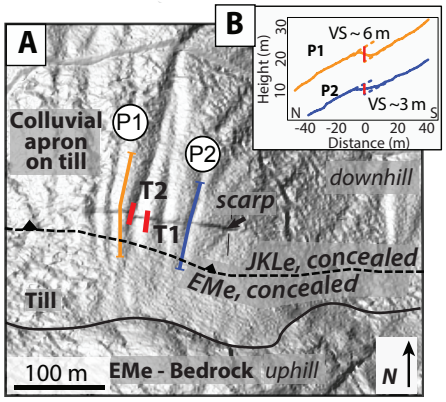

Figure 2. **A.** Hillshade of bare-earth lidar topography (James et al., 2010) showing location of trench 1 (T1) and trench 2 (T2) and geologic setting of fault scarp. EMe, Eocene Metchosin Fm; JKLe, Jurassic-Cretaceous Leech River Complex. **B.** Vertical separations (VS) measured across the fault scarp from Morell et al. (2017). Lidar profiles P1 (interfluve) and P2 (channel) from locations shown in part A.

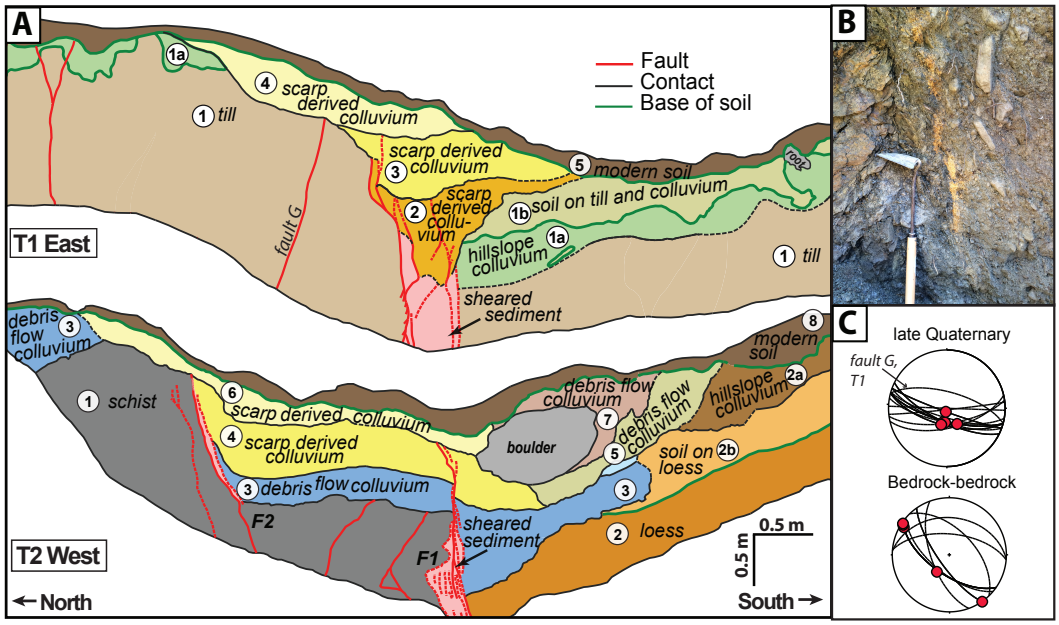

Figure 3. **A.** Simplified trench log for the east wall of trench 1 (T1) and the west wall of trench 2 (T2). Dashed contacts and faults are approximated. For easy comparison with T1 east, T2 west is shown as the mirror image of the trench wall (i.e. eastward view). F1 denotes fault 1 and F2 denotes fault 2. **B.** Field photo from a portion of the west wall of T2 F2, showing vertically-oriented clast in unit 4 and orange gouge. Photo is shown as mirror image (i.e. eastward view) for comparison to part A. **C.** Stereonets show slickenline data on faults that cut late Quaternary sediments, and bedrock-bedrock faults from both trenches. Fault G structural measurement from west wall of T1 (See Fig. S2).

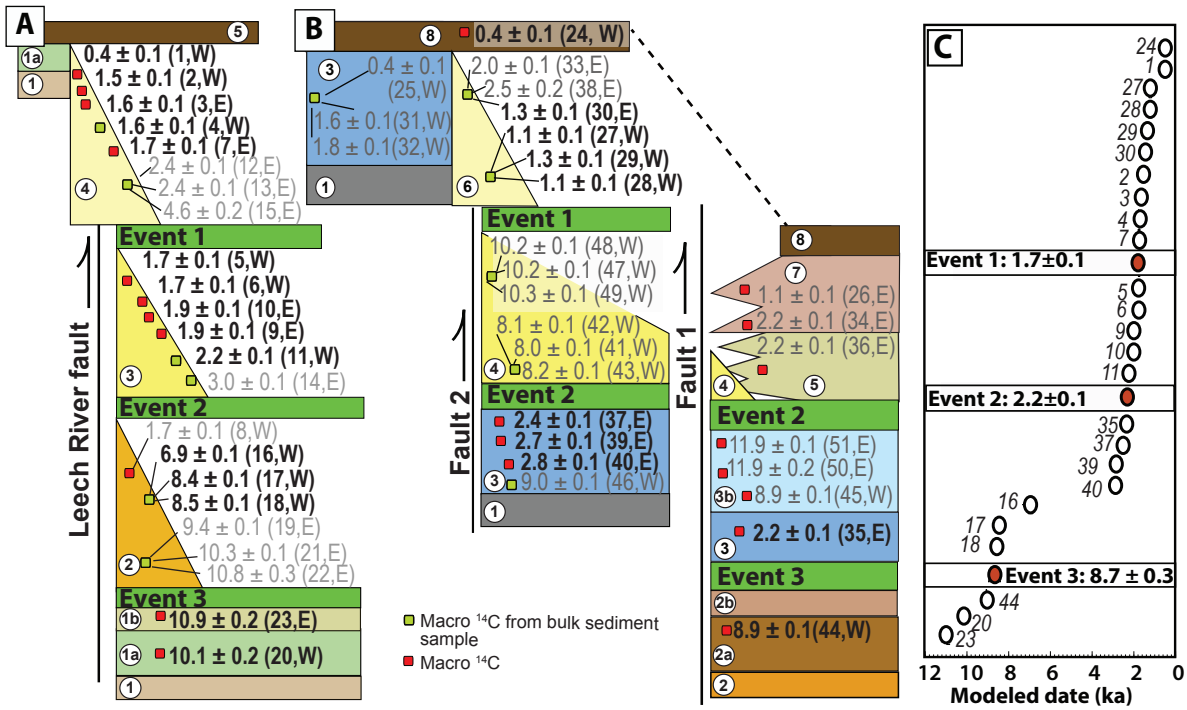

Figure 4. Diagram showing mean and 2σ calibrated radiocarbon ages in trench 1 (Part A) and trench 2 (Part B), in thousands of calendar years before present (ka). Unit numbers (circled) and colors refer to units in Fig. 3A. Ages shown in grey were excluded from the OxCal model shown in Part C. Sample numbers are shown in parentheses, followed by whether the sample was collected from the east (E) or west (W) wall of the trench. Radiocarbon ages (reported following Stuiver & Polach, 1977) from AMS dating were calendar calibrated from radiocarbon ages using OxCal software v.4.3.2 (Bronk Ramsey, 2009) and the IntCal 13 calibration curve (Reimer et al., 2013). **C.** Simplified diagram of OxCal model used to constrain event ages (red dots) from radiocarbon dates of samples from T1 and T2 (white dots). Numbers indicate sample numbers as in Part A. Earthquake ages shown in thousands of calendar years before present (ka). See SI for full details of sampling, OxCal model and radiocarbon ages.

References

Bai, Y., Lay, T., Cheung, K. F., & Ye, L. (2017). Two regions of seafloor deformation generated the tsunami for the 13 November 2016, Kaikoura, New Zealand earthquake. *Geophysical Research Letters*. doi: 10.1002/2017GL073717

Balfour, N., Cassidy, J., Dosso, S., & Mazzotti, S. (2011). Mapping crustal stress and strain in southwest British Columbia. *Journal of Geophysical Research: Solid Earth (1978–2012)*, *116*(B3).

Barrie, V., & Greene, H. G. (2018). An Active Cascadia Upper Plate Zone of Deformation, Pacific Northwest of North America. *Sedimentary Geology*. doi: 10.1016/j.sedgeo.2017.12.018

Bellier, O., & Zoback, M. L. (1995). Recent state of stress change in the Walker Lane zone, western Basin and Range province, United States. *Tectonics*, *14*(3), 564–593.

Bennett, S., DuRoss, C., Gold, R., Briggs, R., Personius, S., Reitman, N., ... Odum, J. (2018). Paleoseismic Results from the Alpine Site, Wasatch Fault Zone: Timing and Displacement Data for Six Holocene Earthquakes at the Salt Lake City-Provo Segment Boundary. *Bulletin of Seismological Society of America*. doi: 10.1785/0120160358

Bronk Ramsey, C. (2009). Bayesian analysis of radiocarbon dates. *Radiocarbon*, *51*(1), 337–360.

Clague, J. J., & James, T. S. (2002). History and isostatic effects of the last ice sheet in southern British Columbia. *Quaternary Science Reviews*, *21*(1), 71–87.

Farías, M., Comte, D., Roecker, S., Carrizo, D., & Pardo, M. (2011). Crustal extensional faulting triggered by the 2010 Chilean earthquake: The Pichilemu Seismic Sequence. *Tectonics*, *30*(6).

Graham, A. (2018). *Geometry, kinematics, and Quaternary activity of the Leech River fault zone, southern Vancouver Island, British Columbia, Canada* (Unpublished master's thesis). University of Victoria, Victoria, BC, Canada.

Halchuk, S., Allen, T., Adams, J., & Rogers, G. (2015). Fifth generation seismic hazard model input files as proposed to produce values for the 2015 national building code of Canada. *Geological Survey of Canada Open File 7576*. http://geogratis.gc.ca/api/en/nrcan-rncan/ess-sst/bc920b71-fa88-537e-80d5-cbfc87b9a9c0.html. doi: 10.4095/293907

Hata, Y., Goto, H., & Yoshimi, M. (2016). Preliminary analysis of strong ground motions in the heavily damaged zone in Mashiki town, Kumamoto, Japan, during the mainshock of the 2016 Kumamoto earthquake (M_w 7.0) observed by a dense seismic array. *Seismological Research Letters*, *87*(5). doi: 10.1785/0220160107

Hetzel, R., & Hampel, A. (2005). Slip rate variations on normal faults during glacial–interglacial changes in surface loads. *Nature*, *435*(7038), 81–84.

James, T., Bednarski, J., Rogers, G., & Currie, R. (2010). LiDAR and digital aerial imagery of the Leech River Fault Zone and coastal regions from Sombrio Point to Ten Mile Point, southern Vancouver Island, British Columbia. *Geological Survey of Canada, Open File 6211*. doi: 10.4095/285486

Lienkaemper, J. J., & Ramsey, C. B. (2009). OxCal: Versatile tool for developing paleoearthquake chronologies–A primer. *Seismological Research Letters*, *80*(3), 431–434.

Massey, N. W. D., MacIntyre, D., Desjardins, P., & Cooney, R. (2005). *Digital geology map of British Columbia*. BC Ministry of Energy and Mines, Geological Survey Branch.

McCaffrey, R. (1996). Slip partitioning at convergent plate boundaries of SE Asia. *Geological Society, London, Special Publications*, *106*(1), 3–18.

McCalpin, J. P., & Hart, E. W. (2002). Ridge-top spreading features and relationship to earthquakes, San Gabriel Mountains Region, Southern California: Part

A. Distribution and description of ridge-top depressions (sackungen): Part B. Paleoseismic investigations of ridge-top depressions. *Ridge-Top Spreading in California: California Geological Survey, Open-File Report*, *1*.

McCalpin, J. P. (2009). *Paleoseismology* (Vol. 95). Academic press.

Morell, K. D., Regalla, C., Leonard, L. J., Amos, C., & Levson, V. (2017). Quaternary Rupture of a Crustal Fault beneath Victoria, British Columbia, Canada. *GSA Today*, *27*(3).

Nelson, A. R., Johnson, S. Y., Kelsey, H. M., Wells, R. E., Sherrod, B. L., Pezzopane, S. K., ... Bucknam, R. C. (2003). Late Holocene earthquakes on the Toe Jam Hill fault, Seattle fault zone, Bainbridge Island, Washington. *GSA Bulletin*, *115*(11), 1388–1403.

Nelson, A. R., Personius, S. F., Wells, R. E., Schermer, E. R., Bradley, L., Buck, J., & Reitman, N. (2017). Holocene Earthquakes of Magnitude 7 during Westward Escape of the Olympic Mountains, Washington. *Bulletin of the Seismological Society of America*, *107*(5), 2394. doi: 10.1785/0120160323

Pánek, T., & Klimeš, J. (2016). Temporal behavior of deep-seated gravitational slope deformations: a review. *Earth-science reviews*, *156*, 14–38.

Personius, S. F., Briggs, R. W., Nelson, A. R., Schermer, E. R., Maharrey, J. Z., Sherrod, B. L., ... Bradley, L.-A. (2014). Holocene earthquakes and right-lateral slip on the left-lateral Darrington–Devils Mountain fault zone, northern Puget Sound, Washington. *Geosphere*, *10*(6), 1482–1500.

Reimer, P. J., Bard, E., Bayliss, A., Beck, J. W., Blackwell, P. G., Ramsey, C. B., ... others (2013). IntCal13 and Marine13 radiocarbon age calibration curves 0–50,000 years cal BP. *Radiocarbon*, *55*(4), 1869–1887.

Reitman, N. G., Bennett, S. E., Gold, R. D., Briggs, R. W., & DuRoss, C. B. (2015). High-resolution trench photomosaics from image-based modeling: Workflow and error analysis. *Bulletin of the Seismological Society of America*, *105*(5).

Sherrod, B. L., Barnett, E., Schermer, E., Kelsey, H. M., Hughes, J., Foit, F. F., ... Hyatt, T. (2013). Holocene tectonics and fault reactivation in the foothills of the north Cascade Mountains, Washington. *Geosphere*, 827–852. doi: 10.1130/GES00880.1

Stuiver, M., & Polach, H. A. (1977). Discussion reporting of ^{14}C data. *Radiocarbon*, *19*(3), 355–363.

Tabor, R. W. (1971). Origin of ridge-top depressions by large-scale creep in the Olympic Mountains, Washington. *Geological Society of America Bulletin*, *82*(7), 1811–1822.

Thompson, S. C., Weldon, R. J., Rubin, C. M., Abdrakhmatov, K., Molnar, P., & Berger, G. W. (2002). Late Quaternary slip rates across the central Tien Shan, Kyrgyzstan, central Asia. *Journal of Geophysical Research: Solid Earth*, *107*(B9). doi: 10.1029/2001JB000596

Toda, S., & Tsutsumi, H. (2013). Simultaneous Reactivation of Two, Subparallel, Inland Normal Faults during the Mw 6.6 11 April 2011 Iwaki Earthquake Triggered by the Mw 9.0 Tohoku-oki, Japan, Earthquake. *Bulletin of the Seismological Society of America*, *103*(2B), 1584–1602.

USGS Quaternary fault and fold database for the United States. (2010). *accessed April 2015.* http//earthquakes.usgs.gov/hazards/qfaults/.

Wells, D. L., & Coppersmith, K. J. (1994). New empirical relationships among magnitude, rupture length, rupture width, rupture area, and surface displacement. *Bulletin of the Seismological Society of America*, *84*(4), 974–1002.

Wilson, J. R., Bartholomew, M. J., & Carson, R. J. (1979). Late Quaternary faults and their relationship to tectonism in the Olympic Peninsula, Washington. *Geology*, *7*(5), 235–239.

Youngs, R. R., & Coppersmith, K. J. (1985). Implications of fault slip rates and earthquake recurrence models to probabilistic seismic hazard estimates. *Bul-*

letin of the Seismological society of America, *75*(4), 939–964.

Figure 1.

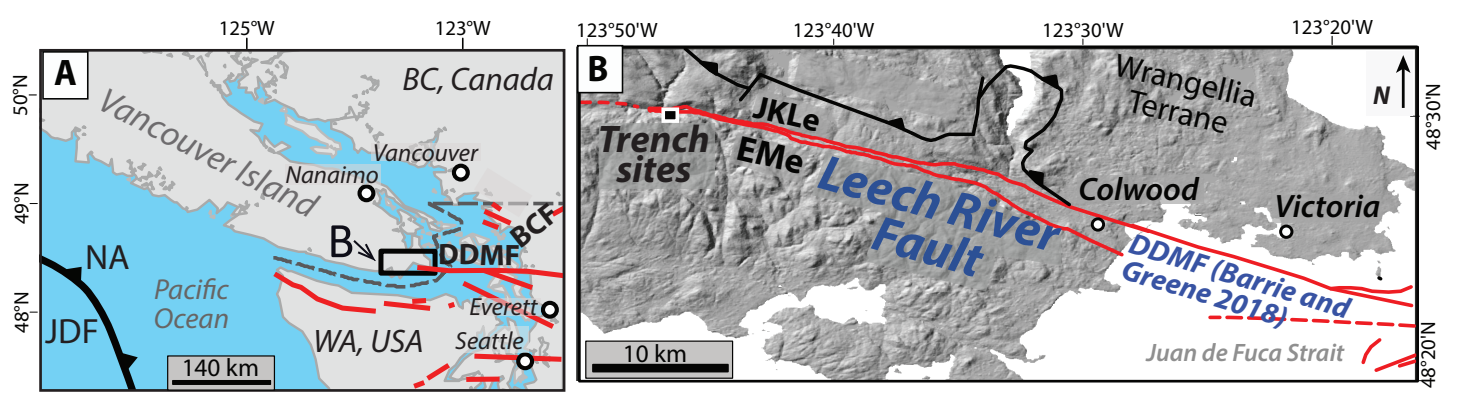
A
125°W
123°W
50°N
49°N
48°N
BC, Canada
Vancouver Island
Nanaimo
Vancouver
B
DDMF
BCF
NA
JDF
Pacific Ocean
Everett
WA, USA
Seattle
140 km
B
123°50'W
123°40'W
123°30'W
123°20'W
48°30'N
48°20'N
N
Trench sites
JKLe
EMe
Leech River Fault
Wrangellia Terrane
Colwood
Victoria
DDMF (Barrie and Greene 2018)
Juan de Fuca Strait
10 km

Figure 2.

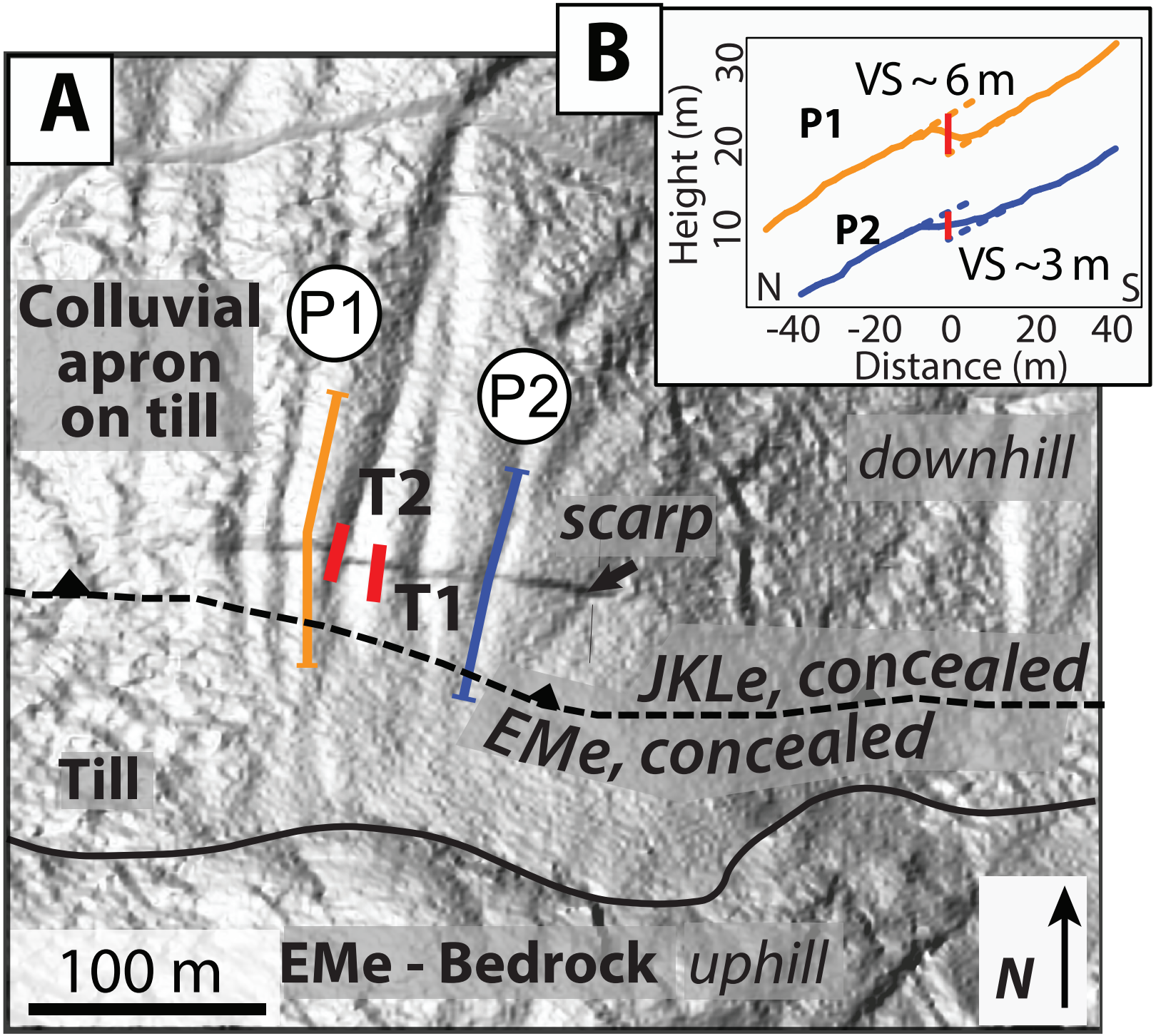
A
B
Colluvial apron on till
P1
P2
T2
T1
scarp
downhill
JKLe, concealed
EMe, concealed
Till
100 m
EMe - Bedrock
uphill
N
Height (m)
10
20
30
VS ~ 6 m
P1
P2
VS ~3 m
N
S
-40
-20
0
20
40
Distance (m)

Figure 3.

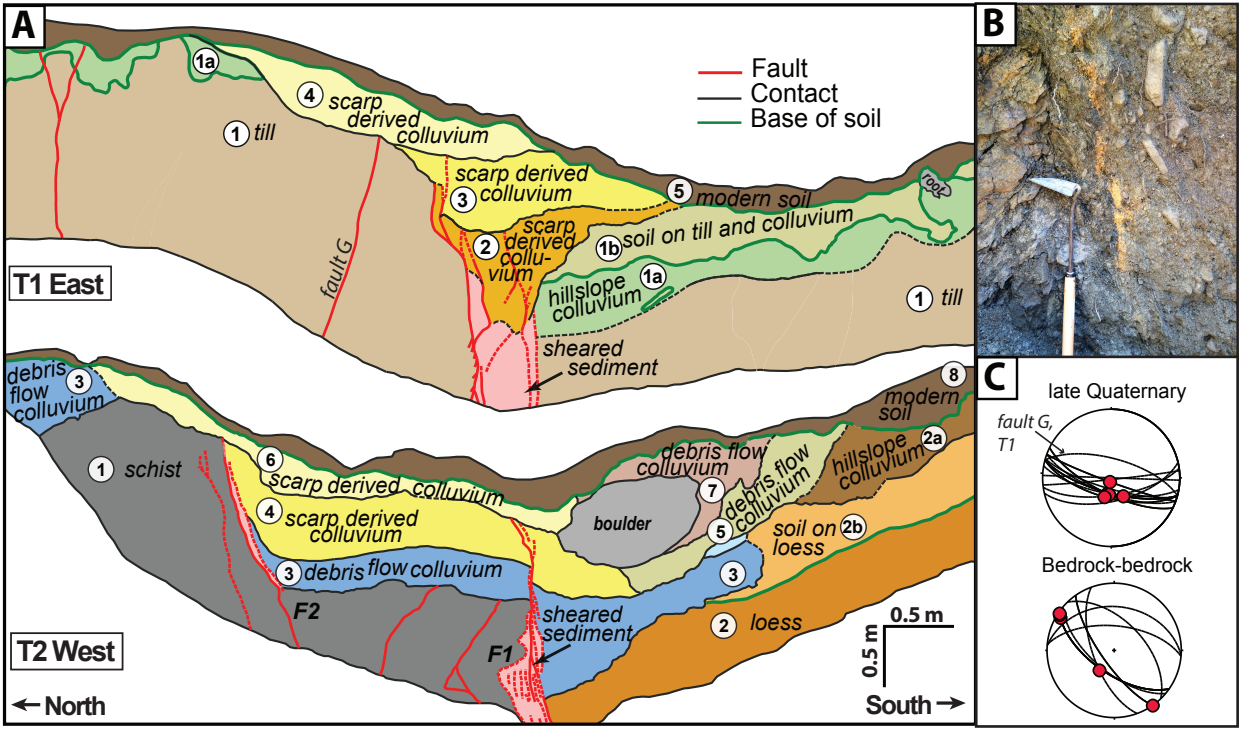
A
B
C
Fault
Contact
Base of soil
T1 East
T2 West
1 till
1a
4 scarp derived colluvium
3 scarp derived colluvium
5 modern soil
2 scarp derived colluvium
1b soil on till and colluvium
1a hillslope colluvium
fault G
root
sheared sediment
debris flow colluvium
3
1 schist
6 scarp derived colluvium
4 scarp derived colluvium
3 debris flow colluvium
F2
F1
sheared sediment
boulder
7 debris flow colluvium
5 debris flow colluvium
8 modern soil
2a hillslope colluvium
soil on loess 2b
3
2 loess
0.5 m
0.5 m
← North
South →
late Quaternary
fault G, T1
Bedrock-bedrock

Figure 4.

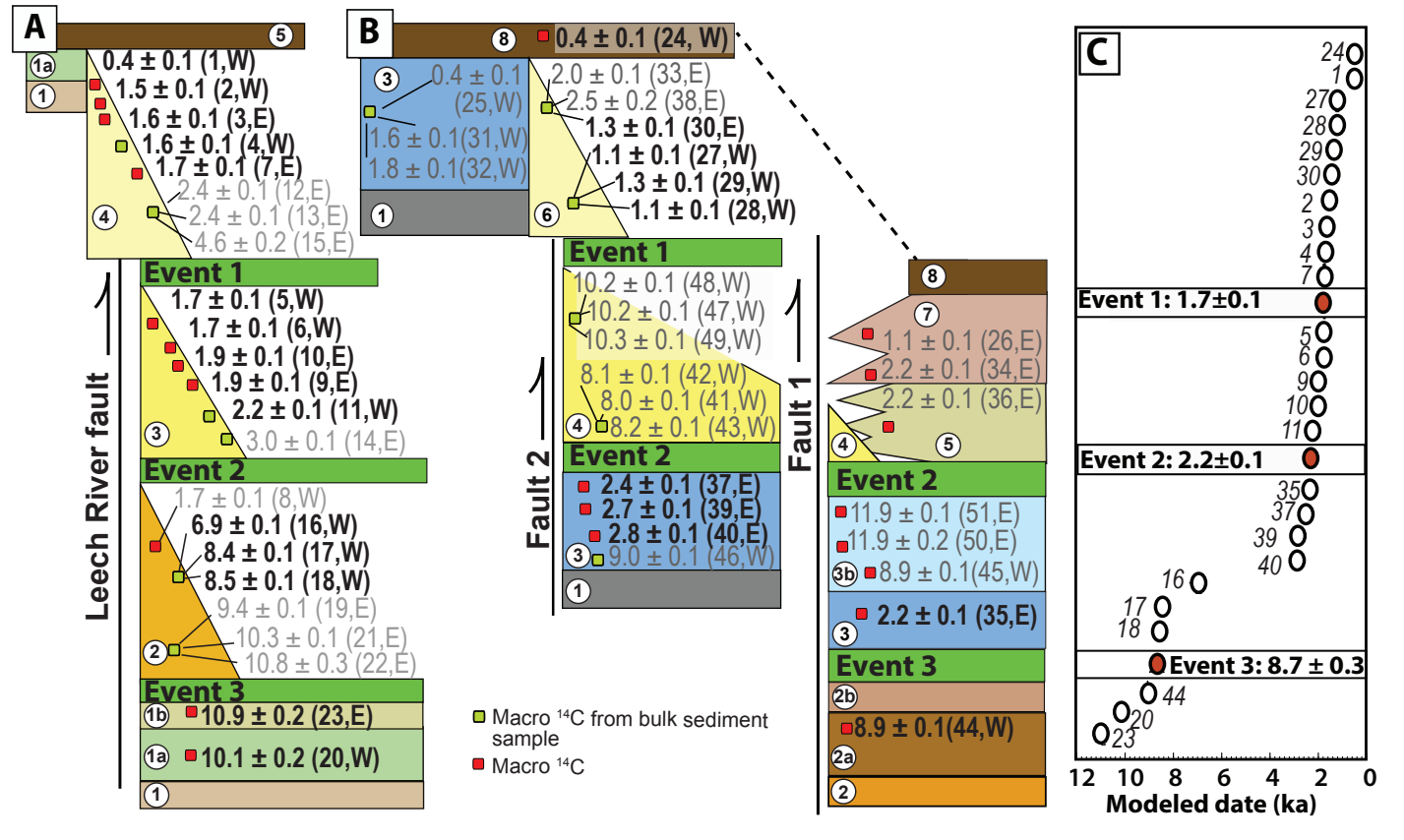
A
5
1a
1
0.4 ± 0.1 (1,W)
1.5 ± 0.1 (2,W)
1.6 ± 0.1 (3,E)
1.6 ± 0.1 (4,W)
1.7 ± 0.1 (7,E)
2.4 ± 0.1 (12,E)
4
2.4 ± 0.1 (13,E)
4.6 ± 0.2 (15,E)
Event 1
1.7 ± 0.1 (5,W)
1.7 ± 0.1 (6,W)
1.9 ± 0.1 (10,E)
1.9 ± 0.1 (9,E)
2.2 ± 0.1 (11,W)
3
3.0 ± 0.1 (14,E)
Event 2
1.7 ± 0.1 (8,W)
6.9 ± 0.1 (16,W)
8.4 ± 0.1 (17,W)
8.5 ± 0.1 (18,W)
9.4 ± 0.1 (19,E)
2
10.3 ± 0.1 (21,E)
10.8 ± 0.3 (22,E)
Event 3
1b
10.9 ± 0.2 (23,E)
1a
10.1 ± 0.2 (20,W)
1
Leech River fault
B
8
0.4 ± 0.1 (24, W)
3
0.4 ± 0.1 (25,W)
1.6 ± 0.1(31,W)
1.8 ± 0.1(32,W)
2.0 ± 0.1 (33,E)
2.5 ± 0.2 (38,E)
1.3 ± 0.1 (30,E)
1.1 ± 0.1 (27,W)
1.3 ± 0.1 (29,W)
1.1 ± 0.1 (28,W)
1
6
Event 1
10.2 ± 0.1 (48,W)
10.2 ± 0.1 (47,W)
10.3 ± 0.1 (49,W)
8.1 ± 0.1 (42,W)
8.0 ± 0.1 (41,W)
4
8.2 ± 0.1 (43,W)
Event 2
2.4 ± 0.1 (37,E)
2.7 ± 0.1 (39,E)
2.8 ± 0.1 (40,E)
3
9.0 ± 0.1 (46,W)
1
Fault 2
Fault 1
8
7
1.1 ± 0.1 (26,E)
2.2 ± 0.1 (34,E)
2.2 ± 0.1 (36,E)
4
5
Event 2
11.9 ± 0.1 (51,E)
11.9 ± 0.2 (50,E)
3b
8.9 ± 0.1(45,W)
3
2.2 ± 0.1 (35,E)
Event 3
2b
8.9 ± 0.1(44,W)
2a
2
Macro 14C from bulk sediment sample
Macro 14C
C
24
1
27
28
29
30
2
3
4
7
Event 1: 1.7±0.1
5
6
9
10
11
Event 2: 2.2±0.1
35
37
39
40
16
17
18
Event 3: 8.7 ± 0.3
44
20
23
12
10
8
6
4
2
0
Modeled date (ka)

Table 1. Mean fault displacement magnitudes and slip rates at trench 1 (T1) and trench 2 (T2)

Interval	T1			T2		
	Fault slip[a]	Wedge height[b]	Vertical separation[c]	Fault slip[a]	Wedge height[b]	Vertical separation[c]
Displacement (m)						
Event 1	0.7 ± 0.5	0.8 ± 0.3	----------	0.9 ± 0.1	1.0 ± 0.3	----------
Event 2	0.5 ± 0.1	1.2 ± 0.2	----------	1.0 ± 0.2	1.0 ± 0.1	----------
Event 3	----------	1.2 ± 0.5	----------	>0.6 ± 0.4	----------	----------
Sum of all events	2.7 ± 0.6[d]	3.2 ± 0.5	5.3 ± 2.0	2.5 ± 0.7	2.0 ± 0.4	4.8 ± 1.2
Slip rate (mm/yr)[e]						
Cumulative	0.2 ± 0.1	0.3 ± 0.1	----------	0.3 ± 0.1	0.3 ± 0.1	----------

a. Sum of fault-parallel offset on all faults. Averaged from both trench walls.

b. Assuming vertical displacements are double the maximum colluvial wedge(s) thickness.

c. From vertical separation of colluvial surface (assuming 60-90º fault dip).

d. Calculated by projecting the top of unit 1 across the fault zone.

e. Determined using earthquake ages in Fig. 4 and methods discussed in text and SI.